

Available online at www.sciencedirect.com

ScienceDirect

journal homepage: www.elsevier.com/locate/he

Degradation prediction of 65 kW proton exchange membrane fuel cells on city buses using a hybrid approach with the advantage actor-critic method

Yujia Zhai ^a, Cong Yin ^{a,b,**}, Renkang Wang ^a, Meiru Liu ^a, Yanzhu Hou ^a, Hao Tang ^{a,b,*}

^a School of Automation Engineering, University of Electronic Science and Technology of China, Chengdu, 610023, China

^b Hydrogen and Fuel Cell Institute, University of Electronic Science and Technology of China, Chengdu 610023, China

HIGHLIGHTS

- Two sets of operating data from commercially operated city buses are employed.
- A hybrid model based on advantage actor-critic (A2C) algorithm is developed.
- The A2C algorithm is applied to predict extracted aging parameters.
- The proposed model can track voltage fluctuations under actual operating conditions.
- A grid search algorithm is used to accelerate the model convergence process.

ARTICLE INFO

Article history:

Received 30 June 2023

Received in revised form

11 August 2023

Accepted 15 August 2023

Available online xxx

Keywords:

Proton exchange membrane fuel cells

Degradation prediction

Advantage actor-critic method

ABSTRACT

Degradation prediction of proton exchange membrane fuel cell (PEMFC) is critical for optimizing fuel cell operation and extending its lifetime, facilitating its large-scale commercialization. This paper proposed a hybrid method based on the mechanism voltage model and the advantage actor-critic (A2C) algorithm to achieve degradation prediction. A semi-empirical voltage model is established to extract four aging parameters: exchange current density, leakage current density, reaction area, and area-specific resistance. A2C is then applied to predict aging parameters and output voltage under stochastic conditions, precisely characterizing the degradation process. Two sets of ~1,000h real data from 65 kW PEMFCs on city buses are used for training, validating, and optimizing the proposed model. The results show that the method can accurately predict voltage degradation and efficiently track voltage fluctuations without delay under actual operating conditions. The prediction root mean square errors for the two datasets with a training ratio 0.8 are 0.0095 and 0.0115, respectively, smaller than conventional prediction methods. The hybrid method can provide detailed internal degradation information and has potential for online forecast applications.

© 2023 Hydrogen Energy Publications LLC. Published by Elsevier Ltd. All rights reserved.

* Corresponding author. School of Automation Engineering, University of Electronic Science and Technology of China, Chengdu, 610023, China.

** Corresponding author. School of Automation Engineering, University of Electronic Science and Technology of China, Chengdu, 610023, China.

E-mail addresses: yincong@uestc.edu.cn (C. Yin), tanghao@uestc.edu.cn (H. Tang).

<https://doi.org/10.1016/j.ijhydene.2023.08.191>

0360-3199/© 2023 Hydrogen Energy Publications LLC. Published by Elsevier Ltd. All rights reserved.

1. Introduction

A fuel cell is a device that generates electricity from chemical reactions and is considered the fourth type of power generation technology after hydroelectric, thermal, and nuclear power [1]. As a highly efficient, environmentally friendly, and low-noise energy conversion technology, fuel cells are the most promising power generation technology with broad applications in aviation, automobiles, and other commercial usages [2]. However, in practical applications, fuel cells face challenges in cost, storage and transportation, reliability, and durability, hindering their large-scale commercialization [3]. The Prognostic and Health Management (PHM) framework is required to address the short lifespan issue and improve the reliability of proton exchange membrane fuel cells (PEMFCs) by monitoring the operating conditions, predicting their health status, and taking appropriate maintenance.

PHM is one of the critical technologies for the commercialization of fuel cell technology [4]. Generally, there are three methods for degradation prediction of PEMFC: model-based, data-driven, and hybrid. The first widely used is model-based, which requires modeling the internal reaction mechanism of the fuel cell. Subsequently, particle filters [5,6] and Kalman filters [7] can be used to predict the internal degradation of the stack. It is challenging to develop a high-precision physical model due to the strong coupling and nonlinearity of the fuel cell system. Therefore, many studies adopt simplified voltage models. Wang et al. [5] considered exchange current density, maximum current density, and polarization resistance during degradation. Zhou et al. [6] constructed a multiparameter physical model covering major internal physical aging phenomena. Ao et al. [7] adopt four voltage degradation models: linear, quadratic, logarithmic, and exponential. Simultaneously, the frequency-domain Kalman filter (FDKF) is presented with less computation time and high accuracy. Khan et al. [8] proposed a dynamic semi-empirical model that uses butterfly optimization algorithms. Many simplified or semi-empirical models do not involve the electrochemical or fluid domain phenomena. Zho et al. [9] constructed a mechanistic model that considers the convective phenomenon of serpentine gas channels and the diffusion phenomenon in the gas diffusion layer. Nematov et al. [10] studied the interaction of water molecules with TiO₂. Balasubramanian et al. [11] investigated the thermodynamic behavior of hydrogen. The degradation mechanisms of fuel cells are complex and extensive. It is challenging to model different stack components mathematically, limiting the effectiveness of model-based prediction methods. With the widespread application of artificial intelligence and machine learning, an alternative means is the data-driven approach.

The data-driven approach can more effectively capture non-linear relationships of degradation data and achieve outstanding predictions. Chang et al. [12] proposed a nonlinear dynamic recurrent neural network (DRNN) method to forecast and estimate remaining useful life (RUL). And the autocorrelation function (ACF) is used to process the model parameters. Liu et al. [13] established Long Short-Term

Memory (LSTM), Support Vector Machine (SVM), and LSTM-SVM composite models for short-term prediction. For the first time, Benaggoun et al. [14] introduced dilated Convolutional Neural Networks (CNNs) for multi-step ahead fuel cell prediction. They developed a Conditional Convolutional Neural Network for long-term forecast, demonstrating better performance in speed and accuracy than the LSTM algorithm. Hua et al. [14] utilized Single Input and Dual Input Echo State Networks (ESNs) to perform prediction with 382h, 1,000h, and 405h, respectively. In Ref. [15], Discrete Wavelet Transform and Ensemble Echo State Network (DWT-EESN) were used to predict Remaining Useful Life (RUL) iteratively. A data-driven Digital twin (DT), a manufacturing approach, was built, and a deep transfer learning model was used in experimental PEMFC deterioration data [16]. It still suffers from over-dependence on data, over-fitting, poor generalization ability, and difficulty in providing internal degradation information, although the method can accurately predict the degradation trend and RUL. Many hybrid prediction methods have been proposed to address the weaknesses of purely data-driven approaches.

The hybrid method combines the advantages of data-driven and model-based approaches. It can provide insight into the degradation process and develop a relatively accurate mathematical model from degradation data. Chen et al. [17] proposed a hybrid method based on wavelet analysis, extreme learning machine (ELM), and genetic algorithm (GA), which considers the influence of load current, relative humidity, and hydrogen pressure in the degradation model. Wang et al. [18] suggested a long-term prediction model based on the Extended Kalman filter (EKF) and Gaussian process regression (GPR). Xia et al. [19] proposed a decomposition-based framework introducing three-dimensional aging factors into the physical model. They applied adaptive extended Kalman filtering (AEKF) and long short-term memory neural networks to predict aging data based on locally weighted regression (LOESS) decomposition. The proposed hybrid prediction approach is shown to outperform single-type methods. To address the challenge of large prediction errors in long-term performance, Wang et al. [20] proposed a fusion prediction strategy that combines a degradation mechanism model with adaptive Brownian bridge-based aggregation LSTM (ABBA-LSTM). The original data is expressed using dimension reduction symbols to improve sensitivity to trends. Though those hybrid methods have addressed the challenges and can predict with high accuracy, there are still issues that need to be discussed further, such as the lack of reliable study based on the long time-scale real-time operating data, shortcomings in the implementation process and the lower voltage fluctuation tracking efficiency due to the stochastic vehicle operating conditions.

Two major limitations of the reported studies are summarized as follows. Firstly, degradation data used in the reported literature are mainly collected under idealized laboratory conditions, which differs from the actual degradation processes in an automotive fuel cell system. We outline some studies on the matter and demonstrate how they fail to account for the complex driving conditions of an actual

vehicle. Some previous studies use the experimental datasets in the IEEE PHM 2014 data challenge [7,18] with a regular interference frequency or Accelerated Stress Test (ATS) aging experiment data [20] with regular load cycles. Other authors attempt to match the actual degradation process by extracting real-time operating condition data to then simulate the actual vehicle driving process [13]. In general, these laboratory settings are simplified and cannot match realistic automotive fuel cell system operations. The operating strategies for urban fuel cell vehicles are far more complex than those simulated in the existing literature. The only study using real data in the literature that we are able to find is Chen et al. [17], which uses 50 h of operating data from an actual electric vehicle. But such a short time span does not meet the long-timescale requirement for a realistic degradation process study. While in this study, two sets of ~1,000h operating data from commercially operated city buses are employed to train the model.

Secondly, the prediction accuracy and response speed under actual operating conditions for long-term degradation prediction still need further improvement. The degradation trend of the selected health indicator can be predicted but lose process details [14,21]. Benagoune et al. [22] can realize multi-step-ahead prediction with small errors but cannot achieve real-time tracking of operating conditions over long time scale without more detailed information of internal degradation.

In this paper, we adopt deep reinforcement learning (DRL) to update and predict state parameters extracted from the voltage model to provide internal degradation details. Among various reinforcement learning algorithms, advantage actor-critic (A2C) can tackle the difficulty in solving continuous action space and stochastic learning strategy of value-based RL. It also reduces variance in obtaining trajectory returns using the advantage function based on the temporal difference to improve training efficiency and stability. Furthermore, it is a dynamic programming process and considers long-term gains in the training process that makes the model response fast to adapt to changing operating conditions. Considering that the parameter changes are continuous processes, a hybrid strategy based on a semi-empirical voltage model and A2C with a continuous action space is proposed to make long-term degradation prediction for PEMFCs. To improve training efficiency and model performance, we used grid search to adjust the hyperparameters of the A2C model automatically. The main contributions of this paper are as follows.

- 1 The PEMFC hybrid degradation prediction model is trained, validated, and optimized using degradation data with ~1000 h from 65 kW fuel cells on two city buses.
- 2 The A2C algorithm based on continuous action space is applied to predict extracted aging parameters, which represent degradation under different operation conditions, providing a more realistic picture of the stack degradation process.
- 3 The proposed model can accurately predict voltage degradation and efficiently track voltage fluctuations under actual operating conditions.
- 4 A grid search algorithm is used to automatically adjust the A2C model hyperparameters, including the action amplitude, the number of neurons, and the training window, to improve training efficiency and model performance.

The remaining parts are organized as follows: Section 2 describes real-world vehicle degradation data sources and the preprocessing process. Section 3 introduces the parameter extraction process and A2C algorithm. Section 4 analyzes the long-term prediction performance of the proposed hybrid strategy. Finally, the conclusion is made in section 5.

2. PEMFC degradation experiment on city buses

2.1. Degradation experiment design

To prove the effectiveness of the proposed hybrid method, the datasets used in this paper are from the commercially operated city buses in Suzhou, China, as shown in Fig. 1(a). Fig. 1(b) and (c) present the bus power system and its structural diagram. The power system mainly comprises a fuel cell stack, lithium battery, motor, and power converter. The electricity generated by the fuel cell charges the lithium battery through a DC/DC converter, and the lithium battery plays a buffering role when the system power demand changes. They work together to drive the motor in different power modes. The installed sensors measure electrical and physical signals. The data is collected by Controller Area Network (CAN) and then packaged and sent through the wireless network each second. Finally, the server parses the received data packets and stores them in the database. The operational data includes the state of charge (SOC), operating current and voltage, gas inlet and outlet pressure, inlet and outlet airflow, and water temperature.

This paper uses the degradation data from two city buses to study the degradation process of fuel cells. The systems are denoted as PEMFC #1 and PEMFC #2. These two datasets were collected from PEMFC #1 and PEMFC #2 from June 24 to October 7, 2020, and July 12, 2021, to January 10, 2022, respectively, with a running time of approximately 1000 h. Both buses are equipped with a 65 kW dual-stack with 280 cells, and the effective reaction area of each cell is 406 cm². In our previous work [23], the hydrogen flow channels on the anode are serpentine to remove liquid water, while the airflow channels on the cathode are straight to reduce gas pressure drop. The specific technical parameters and operating conditions are shown in Table 1. The curves of fuel cell output power and SOC of June 24, 2020 and July 18, 2021, are represented in Fig. 2. The fuel cell needs to charge the lithium battery frequently when the SOC of the lithium battery is below 80% and 60%, respectively, due to the limited capacity of the lithium battery (usually 50 kWh). Generally, varying fuel cell power levels, between 8 kW and 65 kW and 18 kW–65 kW, are set to meet various SOC. It can be observed that the output power of PEMFC #1 and PEMFC #2 is no more than 25 kW and 35 kW, respectively. The operating state is affected by both the actual road conditions and the SOC of the lithium battery, and it is in a dynamic working process of irregular load cycling. Compared with stable operating conditions in laboratory conditions, these actual operational data, with constantly changing operating conditions like current, temperature, and gas flow, are more significant for research.

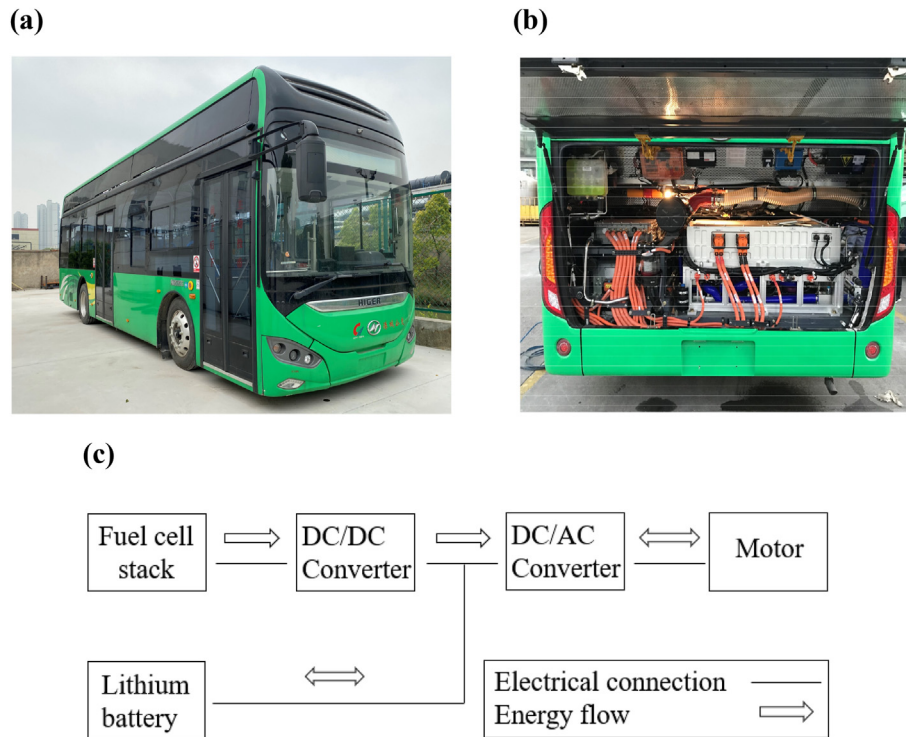


Fig. 1 – PEMFC city bus with hybrid system: (a) City bus, (b) Power system, (c) Structural diagram of power system.

2.2. Data preprocessing

The raw data needs further processing to construct datasets suitable for this study. The original data is massive since the monitoring system collects fuel cell operating data at 1 Hz, which is not conducive to developing the model. Interval sampling of the original data is necessary to reduce computation time and improve prediction efficiency. Considering that the time scale of the internal aging process is in hours, data are sampled every 20 min and any data point of 0 current is removed. It is worth noting that data can only be sampled after 120s of stable operation at a certain operating current point since the system takes some time to reach a stable operating state during the start-up and load-changing processes of the bus. After sampling, the voltage data under specific currents are classified and processed using a moving average to eliminate noise and errors caused by sensors and data acquisition equipment. The data are then be sorted according to the sampling time sequence. The fuel cell components' degradation and road conditions affects the output

voltage variations. The operating status changes dynamically with road conditions. Therefore, the processed data includes much degradation and irregular load cycle information.

The working current and average cell voltage of sampling points of two datasets throughout operation periods are depicted in Fig. 3. The current density of PEMFC #1 is mainly at 40A (0.099 A/cm²), 65A (0.160 A/cm²), 90A (0.222 A/cm²), 120A (0.296 A/cm²), and 150A (0.370 A/cm²), while that of PEMFC #2 is primarily at 90A (0.222 A/cm²), 120A (0.296 A/cm²), 150A (0.370 A/cm²), and 170A (0.419 A/cm²), with a total operating time proportion over 95%. As one of the health indicators of fuel cells, the voltage change trend demonstrates the performance degradation process and contains operational information, such as start/stop, idle, and load-change. PEMFC #1 mainly works at 120A between 440h and 540h, at 90A between 840h and 960h, and has a shorter cumulative operating time at 150A than other currents. And voltage fluctuations increase with time. The voltage fluctuations of PEMFC #2 are less than those of PEMFC #1. Additionally, the difference in the amplitude of the cell voltage between the two sampling points can reach 40 mV, much larger than that caused by the stack internal degradation over the same period of time. Thus, the data complexity and randomness requires the proposed model to be more effective.

Table 1 – Parameters of PEMFC #1 and #2.

| Parameter | Value |
|----------------------------------|----------------------|
| Reaction area (cm ²) | 406 |
| Number of cells | 280 |
| Anode gas pressure (atm) | 1.20–1.30 |
| Cathode gas pressure (atm) | 1.02–1.15 |
| Temperature (°C) | 55–65 |
| Current (A) of PEMFC #1 | 40; 65; 90; 120; 150 |
| Current (A) of PEMFC #2 | 90; 120; 150; 170 |

3. The proposed hybrid prognostics model

This section describes a hybrid prognostics method based on the semi-empirical voltage model and the A2C algorithm, validated with two sets of around 1000 h of real data from the

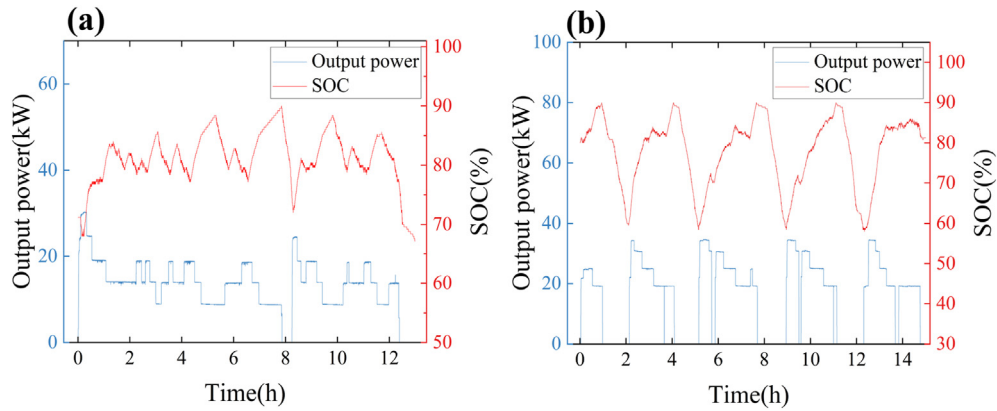


Fig. 2 – Fuel cell output power and SOC of lithium batteries for a given day: (a) PEMFC #1, (b) PEMFC #2.

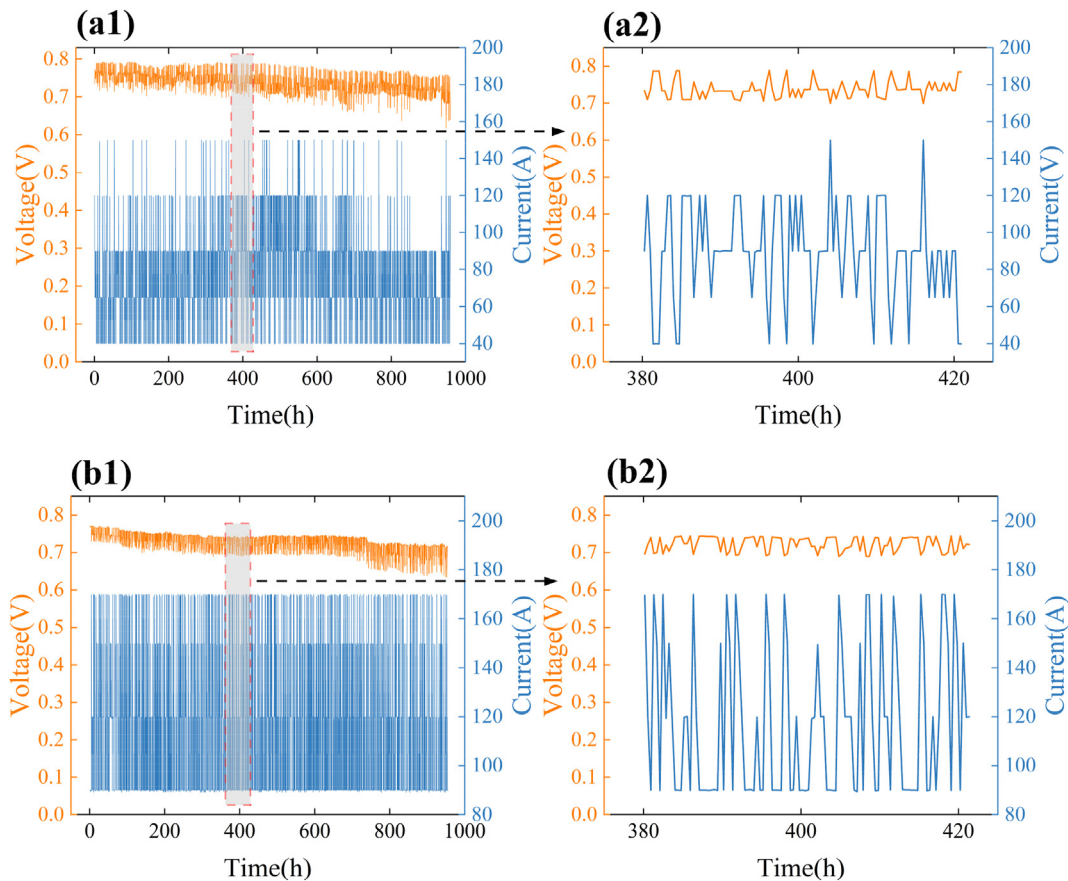


Fig. 3 – Measured output voltage and current of two datasets: (a1) PEMFC #1, (a2) Detailed information of PEMFC #1, (b1) PEMFC #2, (b2) Detailed information of PEMFC #2.

city buses. The proposed model is trained on the training dataset and then completes a long-term prediction task during the testing phase. The implementation framework is shown in Fig. 4. Section 3.1 introduces the semi-empirical voltage degradation model. Four aging parameters are selected based on the operating conditions' influence on the performance degradation. The A2C algorithm with continuous action space is discussed and its implementation details are described in Sections 3.2 and 3.3, respectively.

3.1. Semi-empirical voltage degradation model for feature extraction

Polarization curves indicate the fuel cell's health and degradation trend [24]. However, performing polarization tests on fuel cell stacks installed in city buses is impossible. Instead, a method based on the fuel cell voltage model can be used to decide the aging parameters, and it should reflect the degradation pattern of the stack's internal parameters.

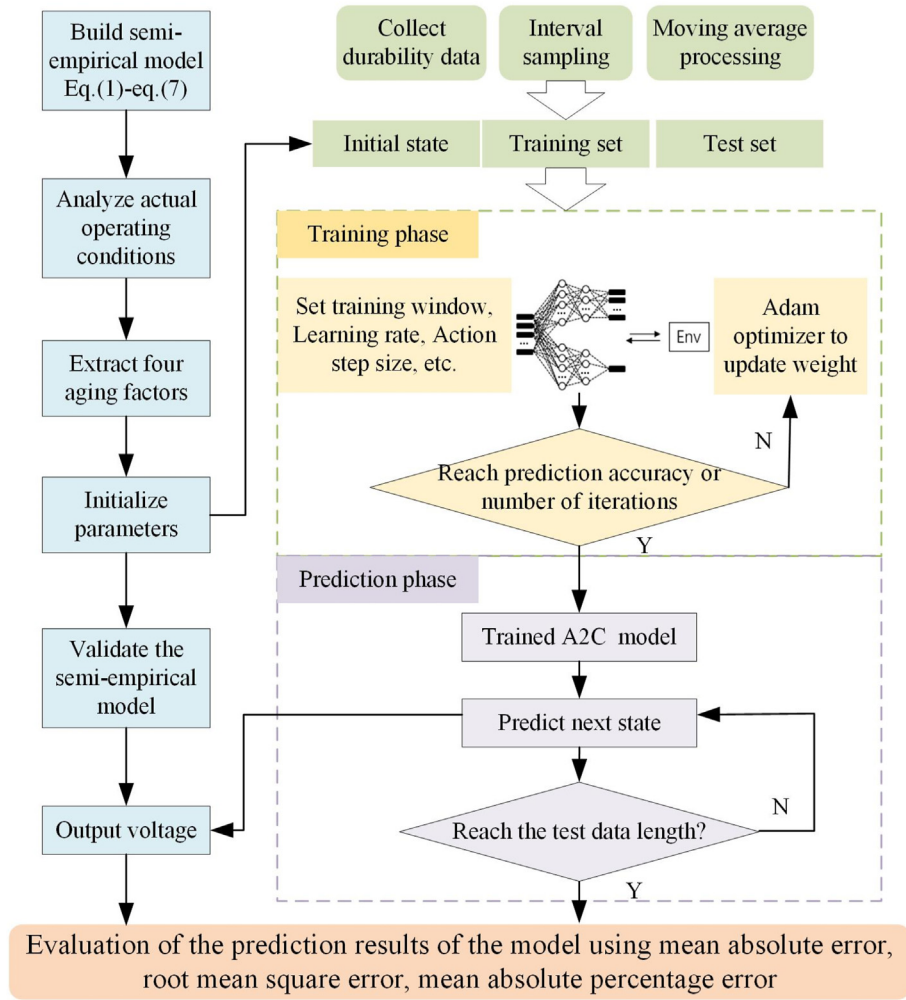


Fig. 4 – Flow diagrams of the proposed hybrid method based on the advantage actor-critic model.

The output voltage reflects the stack performance and decreases as the fuel cell degrades. A semi-empirical voltage model can be established by ignoring cell differences. Typically, the cell output voltage is expressed as [25]:

$$V_{\text{cell}} = V_{\text{thermo}} - V_{\text{irrev}} = V_{\text{thermo}} - V_{\text{act,A}} - V_{\text{act,C}} - V_{\text{ohmic}} - V_{\text{conc,A}} - V_{\text{conc,C}} \quad (1)$$

where V_{thermo} represents the thermodynamic voltage. V_{irrev} is the irreversible voltage loss including the activation, concentration at anode and cathode and ohmic overpotentials. Since the reactant concentration and products in the catalyst layer significantly impacts fuel cell voltage, the pressure loss between the gas inlet and the catalyst layer due to gas convection and diffusion mass transport in the channels is considered when calculating the thermodynamic voltage. It can be calculated as follows [9]:

$$V_{\text{thermo}} = 1.229 - 0.85 \cdot 10^{-3} (T_{\text{cata}} - 298.15) + \frac{RT}{2F} \left(\ln P_{\text{H}_2, \text{cata}} + \frac{1}{2} \ln P_{\text{O}_2, \text{cata}} \right) \quad (2)$$

where T_{cata} is the catalyst layer temperature. $P_{\text{H}_2, \text{cata}}$ and $P_{\text{O}_2, \text{cata}}$ represent H_2 and O_2 pressures at anode and cathode in the catalyst layer, respectively. The gas pressure in the catalyst

layer is the difference between the gas inlet pressure and the pressure drop caused by the gas flow channel and gas diffusion layer. The specific calculation can be found in Ref. [26].

The Butler-Volmer equation describes the exponential relationship between the current and the activation overpotential [27]:

$$j = j_0 \left[\exp \left(\frac{\alpha n F V_{\text{act}}}{RT} \right) - \exp \left(\frac{-(1 - \alpha) n F V_{\text{act}}}{RT} \right) \right] \quad (3)$$

where j represents the working current density, j_0 the exchange current density, n the number of electrons transferred in the electrochemical reaction, $R = 8.314$ the ideal gas constant, $F = 96,485$ the Faraday constant, and α the transport coefficient ranging from 0 to 1. To simplify the model, we assume that the reaction is symmetric and set α to be 0.5 [28]. The formula for the activation overvoltage is rewritten as:

$$V_{\text{act}} = \frac{2RT}{\alpha n F} \sinh^{-1} \left[\frac{j}{2j_0} \right] \quad (4)$$

The activation overpotential in the low current density region is in an approximately linear relationship with the operating current density. Meanwhile, the fuel cell stack studied in this paper mainly operates at low current densities.

The activation overpotential is the primary factor causing the decrease in output voltage, so j_0 is selected as the first internal performance indicator.

The ohmic overpotential expressed by the area-specific resistance is:

$$V_{ohmic} = j(ASR_{ohmic}) \quad (5)$$

where ASR_{ohmic} is the area-specific resistance, which value is related to the thickness and conductivity of the electrolyte. The proton exchange membrane degradation and bipolar plate corrosion can create a resistant surface layer and exacerbate the decline in proton conductivity, resulting in more significant internal resistance. Therefore, ASR_{ohmic} is selected as the second degradation index.

Concentration overpotential can be expressed as an equation:

$$V_{conc} = B_c \ln \frac{j_L}{j_L - j} \quad (6)$$

where B_c is an empirical parameter representing the impact of water and gas accumulation on the current density's non-uniformity of the electrode [28]. j_L is the limiting current density. The equation shows that the concentration loss is small when the working current density is much smaller than the limiting current density. However, when the current density approaches j_L , it can significantly impact the stack's performance, causing a rapid decrease in output voltage. The aging parameters were not extracted from concentration loss since the fuel cells studied in this paper mainly operate in the low current density range. Optimization algorithms can calculate the empirical parameter values and the limiting current density.

A fuel cell electrolyte conducts a small amount of electronic current. As the membrane ages, fuel penetration may occur. Considering the impact of leakage current on the stack performance and ignoring the cathode activation and anode concentration overpotentials [28], the cell output voltage can be rewritten as:

$$V_{cell} = V_{thermo} - \frac{2RT}{\alpha nF} \sinh^{-1} \left[\frac{j + j_{loss}}{2j_0} \right] - j \cdot ASR_{ohmic} - B_c \ln \left(\frac{j_L}{j_L - j} \right) \quad (7)$$

Besides using j_0 and ASR_{ohmic} as aging parameters, leakage current j_{loss} and the reaction area A are also be selected as degradation indicators. The initial values of these four aging parameters for PEMFC #1 and PEMFC #1 are obtained by Particle Swarm Optimization (PSO) algorithm applied to the first-day operating data on June 24, 2020 and July 12, 2021, respectively. These values are listed in Table 2. The semi-empirical degradation voltage model was then validated as presented in Fig. 5.

3.2. Advantage actor-critic method

3.2.1. A2C algorithm with continuous action space

A2C is a combination of policy gradient and value-based reinforcement learning methods. Two neural networks (actor and critic) represent the policy $\pi_\theta(a|s)$ and value function $V_\pi(s)$, respectively. Given the parameter θ of the actor-

Table 2 – Parameter initialization.

| Parameters | PEMFC #1 | PEMFC #2 |
|---------------------------------|-------------------------|-------------------------|
| | Value | Value |
| j_0 (A/cm ²) | 2.2084×10^{-4} | 2.1597×10^{-4} |
| j_{loss} (A/cm ²) | 7.4198×10^{-2} | 7.8603×10^{-2} |
| A (cm ²) | 406 | 406 |
| ASR (Ω·cm ²) | 4.9227×10^{-2} | 1.4200×10^{-2} |

network, the policy function is the process of the actor making decisions on the current state. And the value function is the critic's evaluation of the current actor. The aging parameter degradation process must be transformed into a dynamic programming and sequential decision process. The value of actions represents the parameter trend at the next moment. The trend is described using the policy concept in reinforcement learning, where the state stands for the values of the aging parameters. The four initialized aging parameters is the model's initial state s_0 .

Assuming that the actor and the environment interact multiple times and obtain a particular trajectory $\tau = \{s_1, a_1, s_2, a_2, \dots, s_t, a_t\}$, the probability of this trajectory occurring can be calculated as follows:

$$p_\theta(\tau) = p(s_1) \prod_{t=1}^T p_\theta(a_t|s_t) p(s_{t+1}|s_t, a_t) \quad (8)$$

where the probability $p_\theta(a_t|s_t)$ of taking action a_t in the state s_t is determined by the parameters θ of the actor-network, and the actor reaches a new state s_{t+1} with the probability $p(s_{t+1}|s_t, a_t)$ decided by the environment when taking the same action a_t in the same state s_t . Typically, the environment is fixed, so it is necessary to adjust the parameter θ to obtain trajectories with the maximum possible reward [29]. The total reward $R(\tau)$ for a trajectory τ is obtained by adding the rewards r at each step. $R(\tau)$ is a random variable and the expected reward under the parameters θ can be obtained as follows:

$$\bar{R}_\theta = \sum_{\tau} R(\tau) p_\theta(\tau) \quad (9)$$

Gradient ascent is used to maximize the expected reward:

$$\begin{aligned} \nabla \bar{R}_\theta &= \sum_{\tau} R(\tau) \nabla p_\theta(\tau) \\ &= E_{\tau \sim p_\theta(\tau)} [R(\tau) \nabla \log p_\theta(\tau)] \end{aligned} \quad (10)$$

$R(\tau)$ obtained directly from the trajectory has no bias, but the cumulative reward has a large variance. This high variance is an essential factor leading to overfitting. The advantage function is introduced to address this issue. The gradient formula is shown as follows:

$$\begin{aligned} \nabla J(\theta) &= E_{\pi_\theta} [A^\theta(s_t, a_t) \nabla \log p_\theta(a_t|s_t)] \\ &= E_{\pi_\theta} [(Q_\pi(s_t, a_t) - V_\pi(s_t)) \nabla \log p_\theta(a_t|s_t)] \end{aligned} \quad (11)$$

where $A^\theta(s_t, a_t)$ is the advantage function, representing how well the taken action compares to the average. The objective function is:

$$J(\theta) = E_{\pi_\theta} [A^\theta(s_t, a_t) \times \log p_\theta(a_t|s_t)] \quad (12)$$

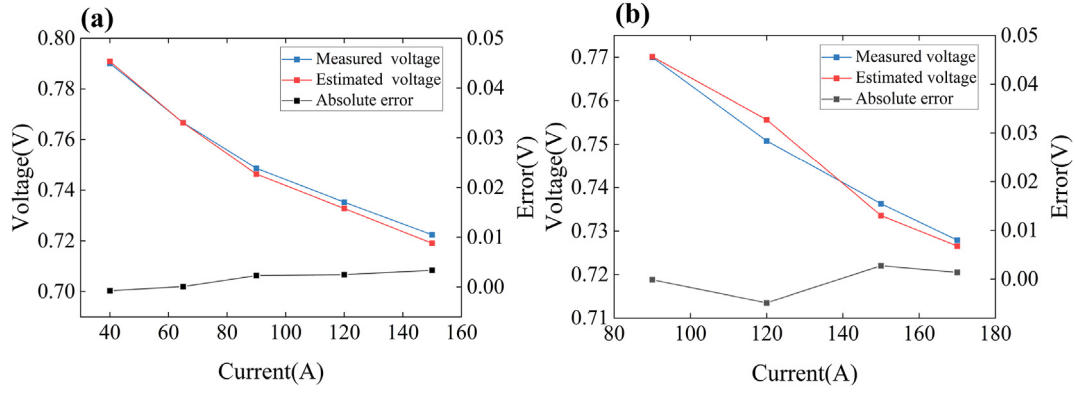


Fig. 5 – Semi-empirical voltage model validation based on initialized aging parameters for (a) PEMFC #1, (b) PEMFC #2.

According to the definition of the state-action and state value functions, the equation can be written as:

$$Q_{\pi}(s_t, a_t) = E[r_t + V_{\pi}(s_{t+1})] \quad (13)$$

In practical applications, the value of the Q function can be directly represented by $r_t + V_{\pi}(s_{t+1})$:

$$J(\theta) = E_{\pi_{\theta}}[(r_t + V_{\pi}(s_{t+1}) - V_{\pi}(s_t)) \nabla \log p_{\theta}(a_t | s_t)] \quad (14)$$

$r_t + V_{\pi}(s_{t+1}) - V_{\pi}(s_t)$ is called the temporal difference (TD) error, an unbiased estimate of the advantage function [30]. From the above equations, only one neural network is needed to estimate the current and following state values, $V_{\pi}(s_{t+1})$ and $V_{\pi}(s_t)$. The reward function defined by the environment is given by:

$$\begin{aligned} \text{reward} &= 10/\text{error} \\ \text{if reward} &> 10 \\ \text{reward} &= 10 \end{aligned} \quad (15)$$

In this study, the variation in the aging factor is continuous, so using the A2C method with continuous action space is in line with the actual situation and theoretically improves training efficiency. The policy network outputs two 4-dimensional vectors representing the mean and variance. We define the probability distribution of each action as a Gaussian distribution according to Eq. (16) and establish four Gaussian distributions. The actor's action to be taken in the current state is obtained by sampling.

$$\pi_{\theta}(a|s) = \frac{1}{\sqrt{2\pi\sigma^2}} e^{-\frac{(x-\mu)^2}{2\sigma^2}} \quad (16)$$

The loss function consists of three components: policy gradient, value, and information entropy losses. It can be obtained by Eq. (16):

$$\log \pi_{\theta}(a|s) = -\frac{(x-\mu)^2}{2\sigma^2} - \log \sqrt{2\pi\sigma^2} \quad (17)$$

As stated in the previous section, the expected reward is maximized using the gradient ascent method. Thus, the strategy gradient loss function should be denoted with a negative sign:

$$\text{policy_loss} = (r_t + V_{\pi}(s_{t+1}) - V_{\pi}(s_t)) \times \left(\frac{(x-\mu)^2}{2\sigma^2} + \log \sqrt{2\pi\sigma^2} \right) \quad (18)$$

The value loss is expressed as:

$$\text{value_loss} = (r_t + V_{\pi}(s_{t+1}) - V_{\pi}(s_t))^2 \quad (19)$$

And the information entropy loss is expressed as:

$$\text{entropy_loss} = \pi_{\theta}(a|s) \log \pi_{\theta}(a|s) = \log \sqrt{2\pi e \sigma^2} \quad (20)$$

Finally, the loss function of the proposed prognostics model is expressed as follows:

$$\text{loss_function} = \text{policy_loss} + \text{value_loss} + \text{entropy_loss} \quad (21)$$

The training process aims to strengthen the actor's decision-making and critic's estimating ability, increasing the probability of actions that lead to higher rewards (higher weights). It first requires the actor with parameters θ to interact with the environment to obtain observation data. Unlike the Monte Carlo method, which waits for the agent and environment to complete a round of interaction to get the total reward before training the network once, the temporal difference-based method can achieve a single-step network update to improve the training efficiency significantly. The update frequency can also be customized, and the implementation details will be discussed in the next section.

3.2.2. Hyperparameter optimization

The model structure described in Section 3.2.1 shows that the number of extracted aging parameters determines the model's input and actor network's output dimensions. The actor neural network outputs the variance and mean. The Softplus activation function is chosen for variance output since the variance must be positive. Like the RELU function, the Softplus function exhibits one-sided inhibition but is relatively smooth. The Tanh activation function is used for the mean output ranging from -1 to 1 . In addition, the number of neurons, the action step size, the training window, and the learning rate must be adjusted to fit the learning task.

This study adopts grid search to implement the automatic parameter tuning process. The time series data is divided into three parts without data leakage: 60% training, 20% validation, and 20% test sets. They are used for model training, parameter tuning, and performance evaluation. It should be noted that the test and validation sets are after the training dataset in time order. Suppose the data is only divided into training and test sets. In that case, the model is adjusted according to test errors instead of validation errors, bringing information from the test set into the model and causing data leakage. It may also lead to a situation where the final score is better than the actual performance and overfitting [31].

We choose three parameters to be optimized including the number of neurons in the hidden layer, training window size, and action amplitude. The chosen parameters take values within given ranges during network parameters optimization process. Theoretically, a larger action amplitude can improve the training efficiency but may also result in an unstable training process and poor model performance. The given parameter combinations are traversed with the pre-determined number of iterations to balance training efficiency and model performance. The set of parameters with the smallest validation mean absolute error is chosen as the optimal solution.

3.3. Implementation of the model

This section elaborates the specific implementation process of the proposed hybrid method based on the theoretical analysis presented in the previous section. The framework is divided into three parts as shown in Fig. 4. The first part elaborates the development of the semi-empirical voltage model (Eq. (1) ~ (8)) and extracts aging parameters based on the fuel cell working mechanism and the data characteristics. An excellent initial state can significantly reduce the exploration time in the action space. The first day data from the two buses are processed separately, and the average voltage at different currents is taken as the target value. PSO is then used to initialize the aging factors and serve as the initial state of the A2C model.

The second part processes the original data and develops an A2C model with continuous action space. The data processing details can be found in Section 2.1. The hyper-parameters are presented in Section 3.2.2. Finally, the model is trained using the processed data of PEMFC #1 and #2.

The third part implements long-term prediction and evaluation of the proposed model. The trained A2C network is used to predict the next state, and then the output voltage is obtained based on the voltage model. In the long-term prediction process, the network forecasts the stack state at any time without updating the network in real time. The predictions will be discussed in the next section.

To visualize the performance of the proposed model, the mean absolute error (MAE), root mean square error (RMSE), and mean absolute percentage error (MAPE) are used as evaluation metrics. These metrics reflect the deviation between the predicted and actual values. The closer the value is to zero, the closer the model's predicted value is to the true value. The calculation process is shown in the following equations:

$$RMSE = \sqrt{\frac{\sum_{i=1}^N (y_i - \hat{y}_i)^2}{N}} \quad (22)$$

$$MAPE = \frac{1}{N} \sum_{i=1}^N \left| \frac{y_i - \hat{y}_i}{y_i} \right| \quad (23)$$

$$MAE = \frac{\sum_{i=1}^N |y_i - \hat{y}_i|}{N} \quad (24)$$

where y_i is the actual voltage, \hat{y}_i is the output, and N is the number of data points in the test set. RMSE is more sensitive to outliers compared to MAE because it has a squared term, while the value calculated by RMSE is generally larger than MAE.

4. Results and discussions

4.1. Prediction of extracted aging parameters

The trained A2C model can forecast the next state despite the current variation. Since the action space is continuous, the actor can take any value within the specified action range to make the model's output approach its actual value. By setting the training ratio to 0.8, there were 2000 training samples for PEMFC #1 and 1986 training samples for PEMFC #2. An excellent initial state of the aging parameters facilitates the model convergence. The initialization is achieved using the PSO algorithm, and the initial values are presented in Section 3.1, which is used as input of A2C. The updated and predicted results are shown in Fig. 6.

Fig. 6 presents the degradation trend of four aging parameters of two fuel cell stacks. Fig. 6(a) shows the irregular variation of the exchange current density of PEMFC #1. There is a slight increase between 780h and 820h, and at the beginning of 400h and 540h, the curve remains at a certain level for a short period. The exchange current density of PEMFC #2 is in an approximately linear decreasing trend shown in Fig. 6(e). But examining the details, we found that the variation at different moments shows apparent irregularity but smaller volatility than Fig. 6(a). Generally, the exchange current density is significantly influenced by reactant concentration, temperature, and catalyst materials. It is known that the actual operating temperature is in a dynamic equilibrium change process. So the decreasing trend is mainly caused by the degradation of the catalyst layer, and the gas transportation issues may result in constant small fluctuations. The percentage changes relative to the initial values are 15.5% and 18.2%, respectively.

The leakage current density of PEMFC #1 and #2 increase approximately linearly, as shown in Fig. 6(b) and (f). Its relative changes to the initial values are 41.2% and 56.4%, respectively. Changes in both exchange current density and leakage current density lead to an increase in activation overpotential and decline in electrochemical activity. Since the activation overpotential is the primary factor causing the decrease in

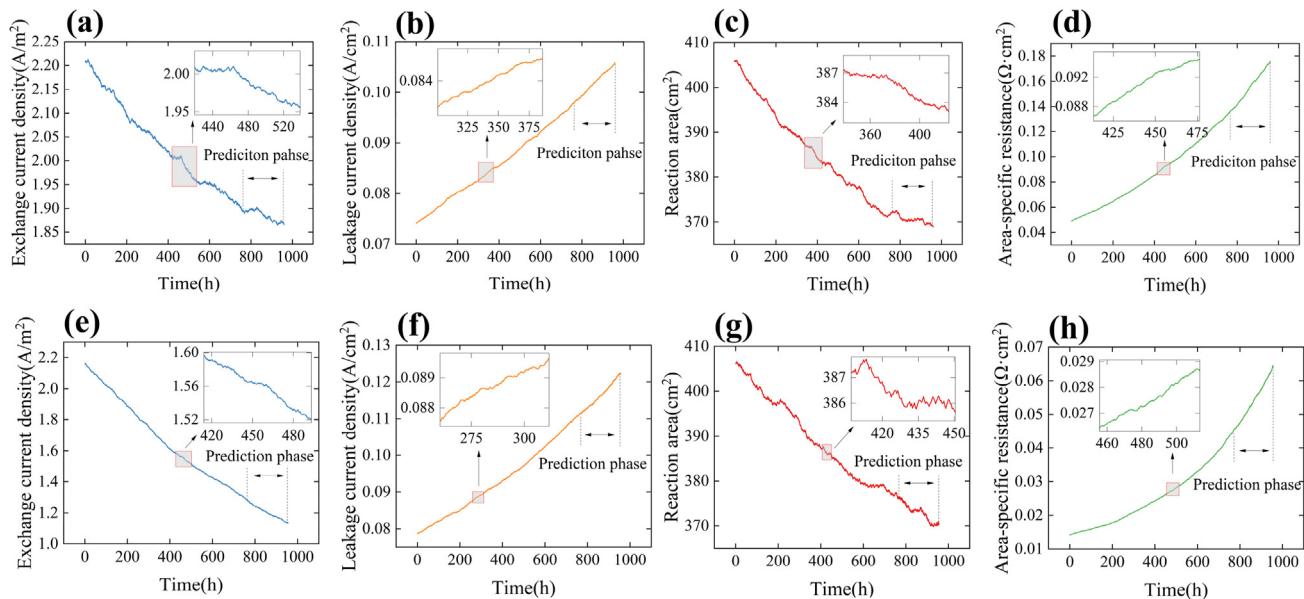


Fig. 6 – Degradation trend of four aging parameters with 80% training data of two datasets: (a) Exchange current density of PEMFC #1, (b) Leakage current density of PEMFC #1, (c) Reaction area of PEMFC #1, (d) Area-specific resistance of PEMFC #1, (e) Exchange current density of PEMFC #2, (f) Leakage current density of PEMFC #2, (g) Reaction area of PEMFC #2, (h) Area-specific resistance of PEMFC #2.

output voltage at low current densities, the two aging parameters significantly impacts the fuel cell performance while operating at low current densities.

The reaction areas of PEMFC #1 and #2 fluctuate downward (refer to Fig. 6(c) and (g)). Despite the wider fluctuation compared with the exchange current density curve, the decline does not vary much across the lifespan. This result is consistent with [32]. In addition, the decrease in the prediction phase becomes flat compared with the training phase, as shown in Fig. 6(c), and the reaction area of PEMFC #2 remains at a certain level between 600h and 690h in Fig. 6(g). The catalyst layer degradation caused by carbon corrosion, excess water (promoting catalyst particle growth), and electrode degradation (causing the decrease of exchange current density [33]) can all lead to a reaction area reduction. The degradation process is also irregular since actual operating conditions are affected by road conditions and environmental factors with a certain degree of complexity and randomness. The relative change from the initial values of the reaction area is 9.4% and 8.9%, respectively.

In Fig. 6(d) and (h), the ASR exhibits an approximately exponential relationship, i.e., the total internal resistance growth rate increases with time. Its effect on the output performance becomes larger as the runtime increases. Similarly, the aging factor associated with total resistance, updated by the AEKF algorithm, shows a smooth increasing trend in Ref. [19]. A decrease in the reaction area and an increase in leakage current density caused by membrane perforation and structural damage of the catalyst layer result in the ASR's increasing trend. When the fuel cell is operated at higher currents, the water produced by the reaction increases the PEM's conductivity, thus reducing the impedance of proton

transport to some extent and introducing fluctuations. In this study, the relative change of the ASR from the initial values is 291% and 364.3%, respectively.

4.2. Prediction of voltage degradation

Based on the results in Section 4.1 and using the semi-empirical voltage model developed in Section 3.1, we are able to obtain the voltage at any given time to get voltage degradation. Due to the randomness of data and the irregularity of the load cycle, it is difficult to predict the fuel cell output voltage directly, and the trained model can only roughly estimate the future voltage resulting in the need for more information. Therefore, we get voltages using the aging parameters updated by the A2C model based on Eq. (7). The model performance is comprehensively evaluated using three metrics: MAE, RMSE, and MAPE. A lower value of these metrics indicates better model performance.

For PEMFC #1, an overall degradation results with different training datasets are shown in Fig. 7(a). The details of the predictions starting at 578h and 770h are shown in Fig. 8(a) and (b). It can be seen that frequent fuel cell voltage changes are caused by frequent changes in working current. PEMFC#1 operates at five currents: 40 A, 65 A, 90 A, 120 A, and 150 A. When the training ratio is set to 0.6, it can be observed in Fig. 8(a) at marker 1 that the predicted values (yellow line) are higher than the true values (blue line) at a certain working current, although the model can track the voltage change trend. When the training ratio is set to 0.8, the predicted values are slightly lower than the true values, as shown in Fig. 8(b) at marker 2. When performing long-term prediction tasks, a lower predicted value than the true value implies that

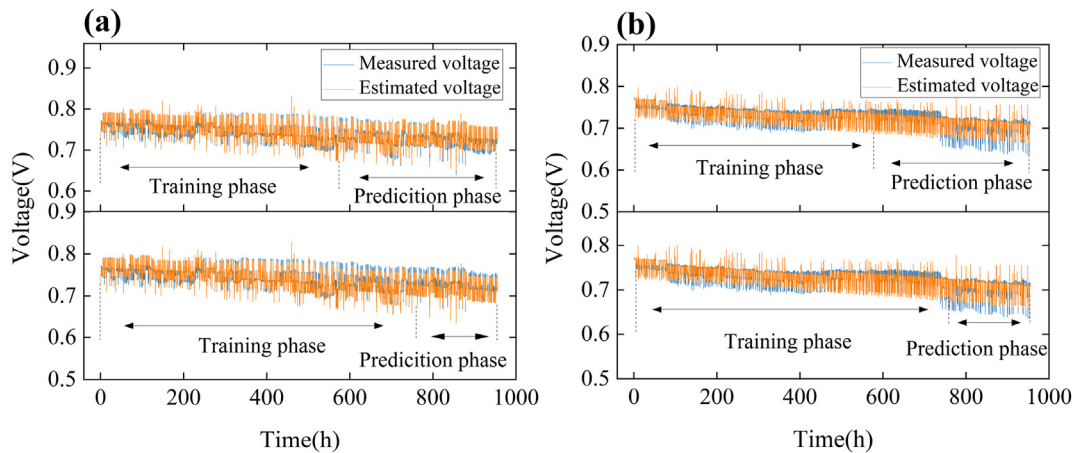


Fig. 7 – Training and predictions with 60% and 80% training data: (a) PEMFC #1, (b) PEMFC #2.

the predicted RUL using voltage drop as the life threshold is less than the actual RUL. Early prediction is more practical as it can give users more time to adjust operating strategies and conditions to slow down fuel cell degradation.

The predictions are quantitatively analyzed by classifying them based on working currents, as shown in Table 3, where num represents the number of test data points, and it is found that the bus works mainly at 40 A, 65 A, and 90 A. The voltage at the same current cannot be obtained directly by collecting data at regular intervals because the working conditions change constantly. Thus, the time distribution at a certain operating current is not uniform. When the training ratio is set to 0.8, the MAE, RMSE, and MAPE values at those currents are no more than 9 mV, 10 mV, and 12%. The MAE, RMSE, and MAPE values at those currents are less than 7 mV, 10 mV, and 10% with a training ratio of 0.6, which is smaller than that in Ref. [21] using the hybrid EKF-LSTM under dynamic conditions. RMSE at 70A and 100A is 19.8 mV and 25.5 mV. Furthermore, it can be observed in Table 3 that the errors do not significantly decrease with an increase in the training samples, primarily because the samples at training ratio 0.6 included 578 h of the operating information, sufficiently enabling the model to capture the dynamic changes and voltage degradation trend. Secondly, a training ratio of 0.6 and a validation ratio of 0.2 were used in the grid search tuning process in Section 3.3. Since the model was not exposed to the last 20% of the data information, the prediction errors at ratio 0.8 may be slightly larger than that at ratio 0.6, which shows the model has good generalization abilities. Additionally, the predictive performance could be better at a current of 120 A, with a significant difference between RMSE and MAE, meaning that there are considerably inaccurate predictions.

For PEMFC #2, although actual road conditions and fuel cell structure significantly differ from PEMFC #1, the proposed method can still accurately predict the degradation and efficiently track the dynamic voltages under load cycling. The results in Fig. 7(b) indicate an overall degradation trend in both

the training and prediction phases. The details of the predictions are shown in Fig. 8 (c) and (d).

The PEMFC #2 operates at four currents: 90A, 120A, 150A, and 170A. The predicted results are classified based on the operating current, as shown in Table 4, revealing that the bus mainly worked at 90A and 120A. The MAE at 90A can reach 5.7 mV though there are situations where the differences between the predicted and actual value are over 30 mV with a training ratio of 0.6. With a ratio of 0.8, the MAE at 90A and 120A are less than 11 mV. We find that the prediction accuracy is relatively high at 90A, 120A, and 150A for both training ratios, while at 170A, the prediction error is rather large. On the one hand, voltage fluctuation increases due to the degradation, making it more difficult to forecast accurately. Furthermore, we observe that the last sampling point of 170A is usually 90A, with a voltage difference of about 40 mV, requiring higher prediction performance. Although the MAE at 170A is greater than 15 mV, it is still possible to rapidly track the downward trend of the voltage when the current changes to 170A. Results show that the proposed model can achieve degradation trend tracking over the entire time scale under actual operating conditions. It provides reference information for the future workload of the fuel cell, making online applications possible.

The proposed hybrid method based on A2C is also compared with other prediction methods in the literature [17,22]. The results of this paper indicate that the model can accurately track high-frequency dynamic changes in voltage. The model performs better than conditional CNN for long-term prediction [22], which can only track the degradation trend ignoring the frequent change of operating conditions. Though in Ref. [17], it can achieve dynamic tracking in the prediction phase using actual operational data, the mean error is larger than that in this paper due to the lack of training samples. Furthermore, its prediction time scale is only 10 h that is much less than 380 h in this paper. During the prediction phase, the network predicts the stack state at any time without updating the network in real time, which raises high

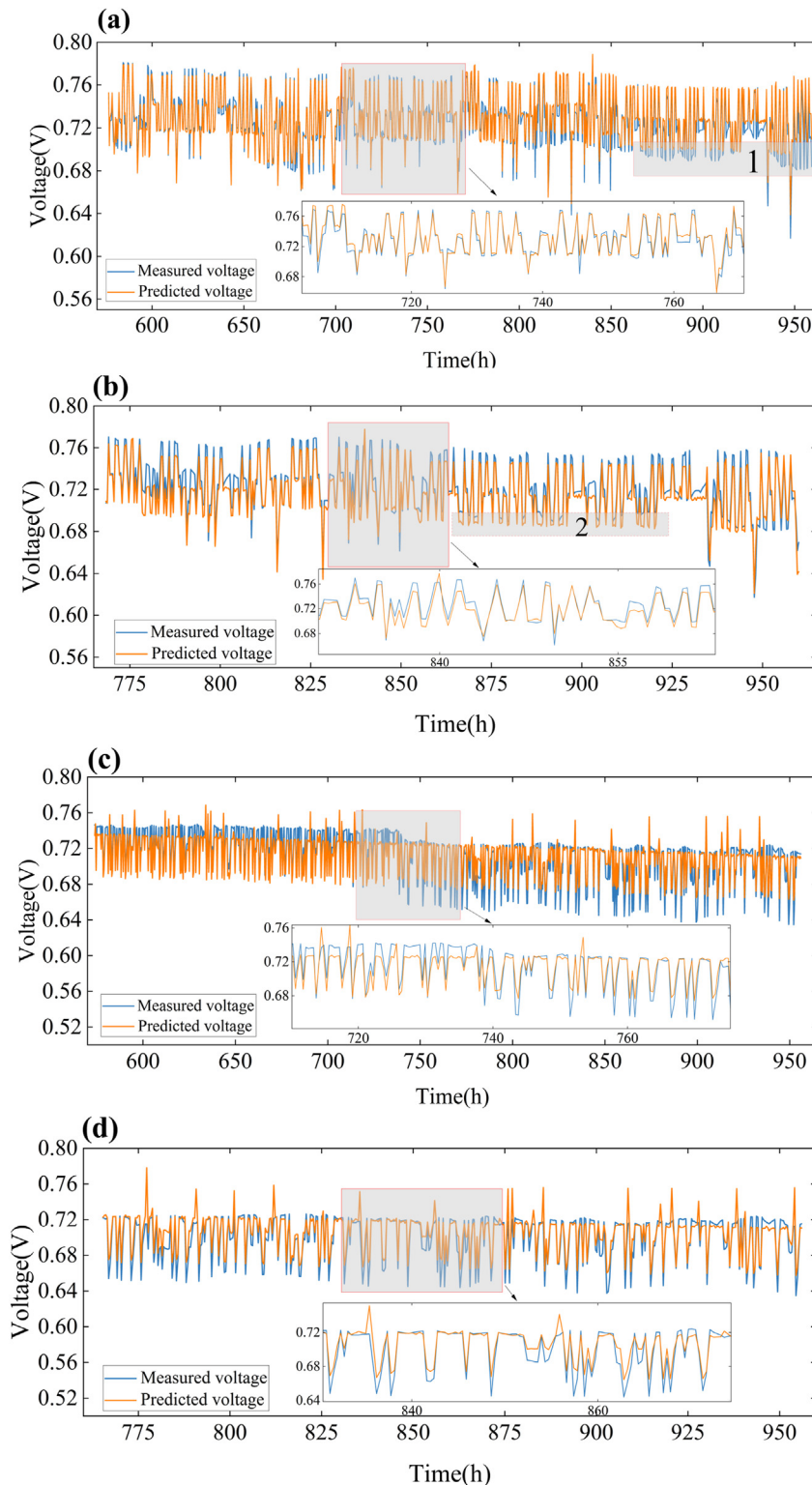


Fig. 8 – The voltage predictions on the training set of two datasets: (a) 60% training data of PEMFC #1, (b) 80% training data of PEMFC #1, (c) 60% training data of PEMFC #2, (d) 80% training data of PEMFC #2.

requirements for model. Fig. 8 shows that the model still has good performance and can capture non-linear changes at any moment whether the output power gets higher or lower in the later part of the forecast. In Fig. 8 (d), when the working current is kept constant, e.g., around 840h or 850h, the model can

also track degradation trends under steady operating conditions, although there are a few data points with large errors. Moreover, based on the quantitative error of two sets, it is known that the model can respond accurately in changes when training samples are sufficient.

Table 3 – Results of PEMFC #1.

| Training ratio | current | | | | |
|----------------|---------|--------|--------|--------|--------|
| 0.8 | 40A | 65A | 90A | 120A | 150A |
| num | 128 | 248 | 178 | 15 | 4 |
| MAE | 0.0086 | 0.0072 | 0.0078 | 0.0118 | 0.0093 |
| RMSE | 0.0095 | 0.0087 | 0.0090 | 0.0151 | 0.0108 |
| MAPE | 0.0113 | 0.0099 | 0.0111 | 0.0179 | 0.0143 |
| Training ratio | current | | | | |
| 0.6 | 40A | 65A | 90A | 120A | 150A |
| num | 201 | 389 | 350 | 77 | 13 |
| MAE | 0.0043 | 0.0068 | 0.0061 | 0.0117 | 0.0055 |
| RMSE | 0.0055 | 0.0094 | 0.0081 | 0.0170 | 0.0083 |
| MAPE | 0.0056 | 0.0093 | 0.0087 | 0.0174 | 0.0084 |

Table 4 – Results of PEMFC #2.

| Training ratio | current | | | |
|----------------|---------|--------|--------|--------|
| 0.8 | 90A | 120A | 150A | 170A |
| num | 282 | 115 | 48 | 50 |
| MAE | 0.0057 | 0.0109 | 0.0068 | 0.0183 |
| RMSE | 0.0099 | 0.0120 | 0.0081 | 0.0190 |
| MAPE | 0.0079 | 0.0158 | 0.0102 | 0.0282 |
| Training ratio | current | | | |
| 0.6 | 90A | 120A | 150A | 170A |
| num | 562 | 206 | 121 | 103 |
| MAE | 0.0081 | 0.0096 | 0.0120 | 0.0157 |
| RMSE | 0.0108 | 0.0109 | 0.0127 | 0.0180 |
| MAPE | 0.0111 | 0.0138 | 0.0173 | 0.0239 |

5. Conclusion

This work developed a novel hybrid prognostic method to achieve long-term degradation prediction of the city bus PEMFC systems. The semi-empirical voltage model and A2C model are employed to predict extracted aging parameters and output voltage during the prediction phase. The main conclusions are as follows:

1. The proposed model is verified with the actual operational data of two city buses. The results show that the model can realize accurate long-term prediction with various working conditions. The MAE of PEMFC #1 and #2 can reach 7.3 mV and 6.9 mA respectively with a training ratio of 0.8, which shows the model's good generalization ability. The accuracy at low operating currents is higher than at high currents. The MAE and MAPE of PEMFC #1 can reach 4.3 mV and 5.6% at 40A, while they can reach 5.7 mV and 7.9% at 90A for PEMFC #2.
2. The operating strategies, internal degradation rates and voltage fluctuations at the same stage vary between two fuel cell systems. The results indicate that the proposed model can both accurately and rapidly track high-frequency dynamic voltage variations up to 40 mV that are larger than those due to degradation over the same

period. It shows better model performance than that of common model-based and data-driven approaches under actual automotive fuel cell system operations load cycle during the whole prediction phase.

3. Four extracted aging factors presents irregular degradation trend with time, which provides more detailed information to analyze the degradation process. The degradation of various parameters is coupled. Results show that the relative change of the ASR is the largest among four parameters, which are 291% and 364.3%, respectively. Its effect on the output performance becomes larger as the runtime increases. The relative changes of leakage current are 41.2% and 56.4%, which has a significant impact on the performance while working at low current density.
4. The aging parameters initialization and automatic tuning of model structure hyperparameters can accelerate the model convergence process to improve the training efficiency. A well initialized state can enable completion of the model training within a few minutes, showing the application potential for online forecast.

In future work, we will further consider the proportional contribution of multiple factors leading to degradation. This may improve long-term predictive performance and prolong the lifespan of fuel cells.

CRedit authorship contribution statement

Yujia Zhai: Methodology, Software, Investigation, Formal analysis, Resources, Writing – original draft. **Cong Yin:** Conceptualization, Formal analysis, Writing – review & editing. **Renkang Wang:** Resources, Investigation. **Meiru Liu:** Methodology, Formal analysis. **Yanzhu Hou:** Resources, Investigation. **Hao Tang:** Conceptualization, Supervision, Writing – review & editing, Project administration, Funding acquisition.

Declaration of competing interest

The authors declare that they have no known competing financial interests or personal relationships that could have appeared to influence the work reported in this paper.

Acknowledgments

This work is sponsored by National Key R&D Program of China (No. 2020YFB1506000), Science and Technology Program of Sichuan Province (No. 2022NSFSC1218) and Science and Technology Program of Suzhou (No. ST202204).

REFERENCES

- [1] Barbir F, Yazici S. Status and development of PEM fuel cell technology. *Int J Energy Res Apr*, 2008;32(5):369–78.

- [2] Laabid A, Saad A, Mazouz M. Integration of renewable energies in mobile employment promotion units for rural populations. *Civil Engineering Journal* 2022;8(7):1406–34.
- [3] Pei P, Chen H. Main factors affecting the lifetime of Proton Exchange Membrane fuel cells in vehicle applications: a review. *Appl Energy* 2014;125:60–75.
- [4] Hua Z, Zheng Z, Pahon E, Péra M-C, Gao F. A review on lifetime prediction of proton exchange membrane fuel cells system. *J Power Sources* 2022;529.
- [5] Wang P, Liu H, Chen J, Qin X, Lehnert W, Shao Z, Li R. A novel degradation model of proton exchange membrane fuel cells for state of health estimation and prognostics. *Int J Hydrogen Energy* 2021;46(61):31353–61.
- [6] Zhou D, Wu Y, Gao F, Breaz E, Ravey A, Miraoui A. Degradation prediction of PEM fuel cell stack based on multiphysical aging model with particle filter approach. *IEEE Trans Ind Appl* Jul-Aug, 2017;53(4):4041–52.
- [7] Ao Y, Laghrouche S, Depernet D, Chen K. Proton exchange membrane fuel cell prognosis based on frequency-domain kalman filter. *Ieee Transactions on Transportation Electrification* Dec, 2021;7(4):2332–43.
- [8] Khan SS, Shareef H, Kandidayeni M, Boulon L, Amine A, Abdennebi EH. Dynamic semiempirical PEMFC model for prognostics and fault diagnosis. *IEEE Access* 2021;9:10217–27. 2021.
- [9] Zhou DM, Nguyen TT, Breaz E, Zhao DD, Clenet S, Gao F. Global parameters sensitivity analysis and development of a two-dimensional real-time model of proton-exchange-membrane fuel cells, vol. 162. *Energy Conversion and Management*; Apr, 2018. p. 276–92.
- [10] Nematov D, Kholmurodov K, Husenzoda M, Lyubchik A, Burhonzoda A. Molecular adsorption of H₂O on TiO₂ and TiO₂: Y surfaces. *Journal of Human, Earth, and Future* 2022;3(2):213–22.
- [11] Balasubramanian R, Abishek A, Gobinath S, Jaivignesh K. Alternative fuel: hydrogen and its thermodynamic behaviour. *J Hum Earth Future* 2022. <https://doi.org/10.28991/HEF-2022-03-02-05>.
- [12] Chang T-J, Cheng SJ, Hsu C-H, Miao JM, Chen S-F. Prognostics for remaining useful life estimation in proton exchange membrane fuel cell by dynamic recurrent neural networks. *Energy Rep* Nov, 2022;8:9441–52.
- [13] Liu Z, Xu SC, Zhao HH, Wang YP. Durability estimation and short-term voltage degradation forecasting of vehicle PEMFC system: development and evaluation of machine learning models. *Appl Energy* Nov, 2022;326.
- [14] Hua Z, Zheng Z, Pahon E, Péra M-C, Gao F. Remaining useful life prediction of PEMFC systems under dynamic operating conditions, vol. 231. *Energy Conversion and Management*; 2021.
- [15] Hua ZG, Zheng ZX, Pahon E, Pera MC, Gao F. Multi-timescale lifespan prediction for PEMFC systems under dynamic operating conditions. *Ieee Transactions on Transportation Electrification* Mar, 2022;8(1):345–55.
- [16] Meraghni S, Terrissa LS, Yue M, Ma J, Jemei S, Zerhouni N. A data-driven digital-twin prognostics method for proton exchange membrane fuel cell remaining useful life prediction. *Int J Hydrogen Energy* Jan 6, 2021;46(2):2555–64.
- [17] Chen K, Laghrouche S, Djerdir A. Degradation model of proton exchange membrane fuel cell based on a novel hybrid method. *Appl Energy* Oct, 2019;252.
- [18] Wang T, Zhou H, Zhu C. A short-term and long-term prognostic method for PEM fuel cells based on Gaussian process regression. *Energies* Jul, 2022;15(13).
- [19] Xia Z, Wang Y, Ma L, Zhu Y, Li Y, Tao J, Tian G. A hybrid prognostic method for proton-exchange-membrane fuel cell with decomposition forecasting framework based on AEKF and LSTM. *Sensors* Dec 24, 2022;23(1).
- [20] Wang C, Dou M, Li Z, Outbib R, Zhao D, Liang B. A fusion prognostics strategy for fuel cells operating under dynamic conditions. *eTransportation* 2022;12.
- [21] Ma R, Xie R, Xu L, Huangfu Y, Li Y. A hybrid prognostic method for PEMFC with aging parameter prediction. *IEEE Transactions on Transportation Electrification* 2021;7(4):2318–31.
- [22] Benagougne K, Yue M, Jemei S, Zerhouni N. A data-driven method for multi-step-ahead prediction and long-term prognostics of proton exchange membrane fuel cell. *Appl Energy* 2022;313.
- [23] Wu D, Li K, Gao Y, Yin C, Song Y, Yang X, Tang H. Experimental and modeling study on dynamic characteristics of a 65 kW dual-stack proton exchange membrane fuel cell system during start-up operation. *J Power Sources* 2021;481.
- [24] Chen J, Zhou D, Lyu C, Lu C. A novel health indicator for PEMFC state of health estimation and remaining useful life prediction. *Int J Hydrogen Energy* Aug 3, 2017;42(31):20230–8.
- [25] Lechartier E, Laffly E, Pera MC, Gouriveau R, Hissel D, Zerhouni N. Proton exchange membrane fuel cell behavioral model suitable for prognostics. *Int J Hydrogen Energy* Jul, 2015;40(26):8384–97.
- [26] Liu M, Wu D, Yin C, Gao Y, Li K, Tang H. Prediction of voltage degradation trend for a proton exchange membrane fuel cell city bus on roads. *J Power Sources* 2021;512.
- [27] Spiegel C. PEM fuel cell modeling and simulation using MATLAB. Elsevier; 2011.
- [28] Larminie J, Dicks A, McDonald MS. Fuel cell systems explained: j. Chichester, UK: Wiley; 2003.
- [29] Kaelbling LP, Littman ML, Moore AW. Reinforcement learning: a survey. *J Artif Intell Res* 1996;4:237–85.
- [30] Konda V, Tsitsiklis J. Actor-critic algorithms. *Adv Neural Inf Process Syst* 1999;12.
- [31] Syarif I, Prugel-Bennett A, Wills G. SVM parameter optimization using grid search and genetic algorithm to improve classification performance. *TELKOMNIKA (Telecommunication Computing Electronics and Control)* 2016;14(4):1502–9.
- [32] Chen H, Zhan ZG, Jiang PX, Sun YH, Liao LW, Wan XB, Du Q, Chen XS, Song H, Zhu RJ, Shu ZH, Li S, Pan M. Whole life cycle performance degradation test and RUL prediction research of fuel cell MEA. *Appl Energy* Mar, 2022;310.
- [33] Jouin M, Gouriveau R, Hissel D, Péra M-C, Zerhouni N. Degradations analysis and aging modeling for health assessment and prognostics of PEMFC. *Reliab Eng Syst Saf* 2016;148:78–95.